Improved New Object Reconstruction with Dynamic Gaussian Splatting

Semester Project Report

Ewa Miazga
ewa.miazga@epfl.ch
Supervisor: Saqib Javed

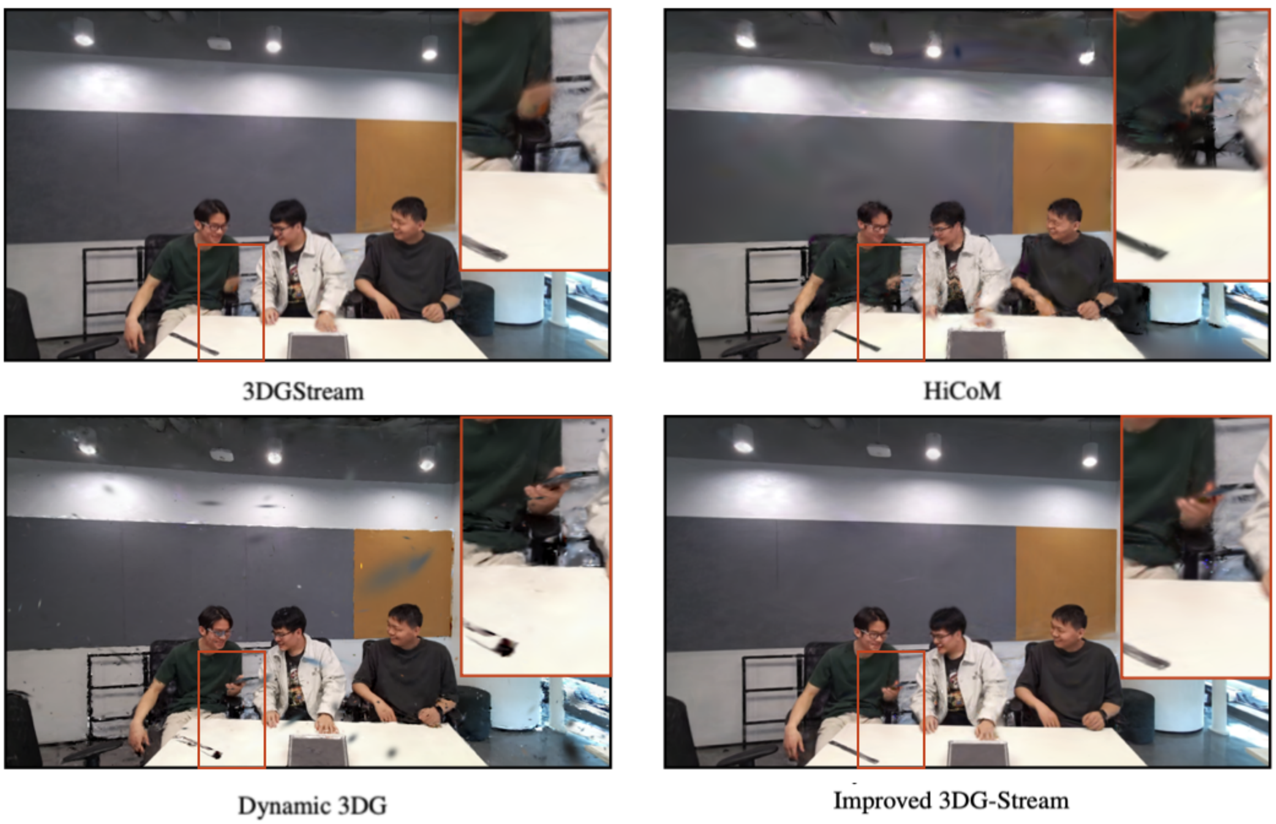

Abstract

Reconstruction of 3D scenes using multi-view cameras remains a significant challenge today. Training is often computationally expensive and does not always guarantee high-quality reconstructions. Furthermore, existing methods may not be suitable for all types of 3D scenes—such as indoor or outdoor environments with many dynamic objects. One notable limitation is the inability to reconstruct objects that emerge after the first frame. Methods like HiCoM and 3DG-Stream rely on a per-frame optimization strategy that is initialized from the first frame, making them unable to model objects that appear later in the sequence. In contrast, Dynamic 3D Gaussian Splatting adopts a frame-to-frame optimization approach, which allows for continuous updates and appears better suited for handling newly emerging elements in dynamic scenes. This work presents both qualitative and quantitative comparisons of the aforementioned methods, focusing on their ability to reconstruct newly appearing objects in dynamic 3D scenes. Additionally, it introduces an improved version of the 3D-Stream method, which demonstrates the capability to reconstruct new objects more effectively.

1. Introduction

Efficient and effective 3D scene representation has the potential to significantly impact various industries, including robotics, gaming, and architecture. In architecture, it could enable interactive, localized modifications to building models and facilitate the generation of novel renderings from arbitrary viewpoints. In the gaming and film industries, it opens the door to dynamic object generation and manipulation for animations. Furthermore, accurate tracking of object motion is essential for applications such as autonomous driving and navigation in unfamiliar environments.

Despite these promising applications, 3D object reconstruction remains vulnerable to real-world challenges and limitations in spatial data acquisition. Current methods fall short in several scenarios. First, achieving high-resolution reconstruction for each frame while maintaining real-time performance is challenging. Second, scenes with multiple moving objects require high-frequency queries to the point cloud, which can lead to prohibitive computational costs per frame. Finally, and perhaps most critically, is the issue of reconstructing objects that appear after the first frame. Although this last challenge may seem trivial, it often results in misleading or incomplete reconstructions. In rendered scenes, these regions may appear partially transparent, revealing background content where newly appeared objects should have been reconstructed.

We ideally would seek to have a method that is able to overcome a challange and reconstruct every object appearing at the scene at any time. Still perserving the qualities of the methods like low storage, fast-rendering and high quality of the rendered output.

2. Dataset

The dataset plays a crucial role in this report, as it must present a fair and consistent challenge to all evaluated methods. It was important that the dataset be both accessible and compatible with the frameworks under test.

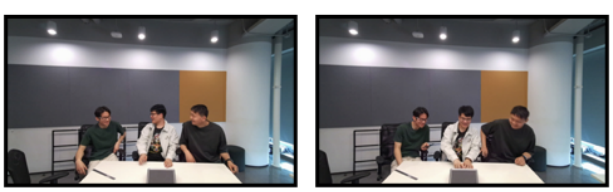

Figure 1. Meetroom dataset example. The individual takes a phone out of his pocket.

The *Meetroom* dataset was captured using a 13-camera multi-view setup. It consists of dynamic scenes recorded at a resolution of 1280×720 and 30 FPS. Specifically, the *discussion* sequence was used for evaluation. It is particularly suitable for testing new object reconstruction, as one of the individuals in the scene takes a phone out of his pocket after a few seconds - making it the primary focus of our evaluation (Figure 1).

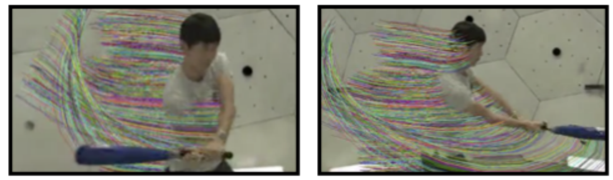

Figure 2. Panoptic dataset example. The batter swings through the air as no ball appears.

The appearance of a new object after the first captured frame was the decisive criterion in dataset selection. During our research, it became evident that datasets containing such characteristics are rarely used in evaluations - representing a significant but often overlooked limitation in existing benchmarks.

For instance, although the *Panoptic* dataset is a standard benchmark for evaluating dynamic Gaussian splatting methods, it does not feature objects that emerge during the sequence (Figure 2). This omission, while perhaps unintentional, can conflict with the logical and expected behavior of individuals in realistic scenes. As such, the evaluation may not reflect the true capabilities of reconstruction frameworks under dynamic conditions.

3. Methods

3.1. 3DGStream [1]

3DG-Stream is an on-the-fly rendering technique designed for fast and efficient free-viewpoint video reconstruction from multi-view video captures. Its key strengths include accelerated training, reduced storage requirements, and high-quality image synthesis.

Initial frame is optimized with 3D Gaussian Splatting technique [2]. Subsequent frames are obtained with two-stage optimization process on previous frame as shown in Figure 3.

Stage 1: Neural Transformation Cache Firstly, each frame passes through the Neural Transformation Cache - a shallow, fully-fused MLP - to obtain the position and rotation of individual gaussians for the consecutive frame.

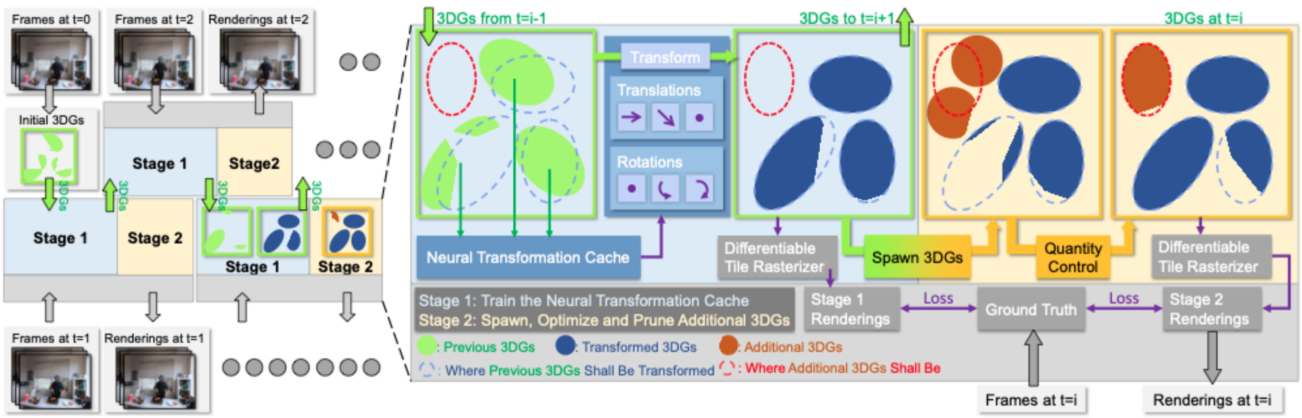

Figure 3. **3DGStream framework**. Reconstruction of 0 frame representation followed by reconstruction of subsequent frame representation using Hierarchical Coherent Motion mechanism and Continual Refinement with new gaussians.

To ensure storage efficiency, the method splits the scene into multi-resolution voxel grids. For each 3D position $\mathbf{x} \in \mathbb{R}^3$, its hash encoding at resolution level ℓ is denoted by:

$$h(\mathbf{x}, \ell) \in \mathbb{R}^d,$$

a d-dimensional feature vector. The function $h(\mathbf{x}, \ell)$ is constructed by an interpolation of the feature vectors at the eight corners of the voxel grid cell that surrounds the point $\mathbf{x}$. The multi-resolution hash encoding is defined as:

$$h(\mathbf{x}) = [h(\mathbf{x}, 0), h(\mathbf{x}, 1), \dots, h(\mathbf{x}, L-1)] \in \mathbb{R}^{Ld},$$

which serves as input to the fully-fused MLP. For a gaussian centered at position $\boldsymbol{\mu}$, the MLP predicts the updates to its translation and rotation (1):

$$\Delta\boldsymbol{\mu}, \Delta\mathbf{q} = \mathrm{MLP}(h(\boldsymbol{\mu})) \tag{1}$$

where $\Delta\boldsymbol{\mu} \in \mathbb{R}^3$ is the translation offset and $\Delta\mathbf{q} \in \mathbb{R}^4$ is the rotation quaternion.

Based on the MLP outputs - translations, rotations, and spherical harmonics (SH) rotation coefficients - the attributes of the gaussians are updated for the subsequent frame.

Loss Function The optimization of Neural Transformation Cache (NTC) parameters for future frames relies on the computation of a loss function between the rendered image and the ground truth. Following the formulation introduced in 3D Gaussian Splatting [2], the loss is defined as a weighted combination of L1 and D-SSIM losses:

$$\mathcal{L} = (1-\lambda)\mathcal{L}_1 + \lambda\mathcal{L}_{\text{D-SSIM}} \tag{2}$$

where $\lambda = 0.2$ is a balancing factor.

The gaussians obtained at the end of Stage 1 are frozen and serve as initialization for the next frame's optimization.

Stage 2: Representing Emerging Objects Stage 2 focuses on modeling newly emerging objects - such as flames, smoke, or liquids - that appear in the scene. These phenomena are not adequately captured by the gaussians inherited from the previous frame. To address this, new gaussians are introduced in frame-specific regions exhibiting poor reconstruction. This ensures that only a minimal number of new gaussians are added, avoiding unnecessary accumulation over time.

Gradient-Based Localization and Adaptation To localize regions where new objects are emerging, the method monitors high view-space positional gradients. These occur when the model attempts - but fails - to approximate unrepresented scene elements using existing gaussians. Since the color attributes of the gaussians are frozen during Stage 1, this leads to large positional updates without photometric improvements.

To handle this, an adaptive 3DG spawning strategy is employed. New gaussians are initialized in high-gradient regions and optimized using the same loss function $\mathcal{L}$ (2).

Furthermore, at the end of each training epoch, an adaptive 3DG quantity control strategy is applied: gaussians in under-reconstructed regions are either deleted or split to enhance spatial coverage and reconstruction quality.

3.2. HiCoM [3]

The method was introduced as learning and storage efficient alternative to the other existing streamable frameworks.

The initalization step optimizes first frame view using 3D Gaussian Splatting [2]. As shown in Figure 4 (a), small

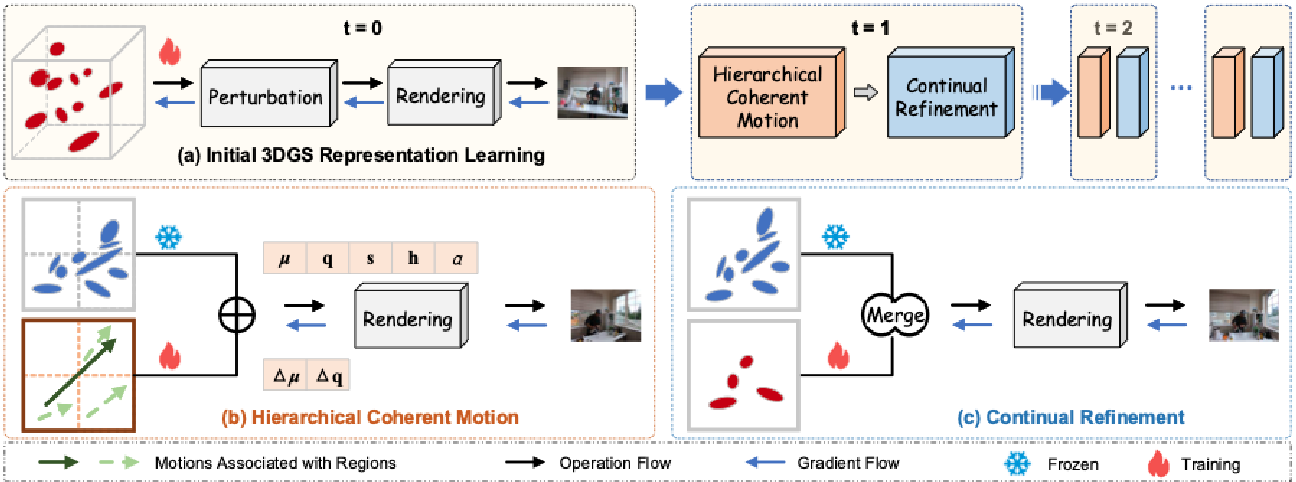

Figure 4. **HiCoM framework**. Reconstruction of 0 frame representation (a), Reconstruction of subsequent frame representation using Hierarchical Coherent Motion mechanism (b), Continual Refinement with new gaussians.

gaussian noise is added to the position attribute of each 3D gaussian. To accomdate for possible overfitting caused by limited access to camera views.

Hierarchical Coherent Model For the next frames the training follows online framework, where the latest view is continuously fetched and used for optimization of current state representation. Then, Hierarchical Coherent Model Figure 4 (b) is used to capture the movement of the gaussians from frame to frame. The model is based on partitioning the space into regions in gradual manner (from more coarse to fine) and then calculating vector $\Delta\mu \in \mathbb{R}^3$ and a quaternion $\Delta q \in \mathbb{R}^4$ for each granulation level. Then for each gaussian we calculate the motion according to formula (3):

$$\Delta\boldsymbol{\mu}_g = \sum_{l=1}^{L} \Delta\boldsymbol{\mu}^l, \quad \Delta\mathbf{q}_g = \sum_{l=1}^{L} \Delta\mathbf{q}^l \tag{3}$$

Continual Refinement Following the motion update of gaussians, 3D Gaussian Splatting is applied to achieve the recent scene renders. However, the hierarchical coherent model is not capable of capturing finer details, especially in the regions with significant gradient changes. There the gaussians are densified and optimized, so the discrepancy betweeen the rendered and target image is reduced. To control the number of gaussians, the same amount that was injected, is removed based on low opacity criterion. The forementioned mechanism is called Continual Refinement and it is shown in Figure 4 (c).

The training in this framework may be done in parallel. Chosen frame t is a referance for k next frames, which makes simultanous training of $\{t+1, \cdots, t+k\}$ possible.

3.3. Dynamic 3D Gaussians [4]

The method combines tasks of dynamic scene reconstruction and tracking of all dense scene elements using multi-view videos with segementation masks.

The first frame is optimized following the 3D Gaussian Splatting method [2]. After the optimization, the gaussians are configured to represent the first frame, including their size, color, opacity, and a background logit that indicates whether a gaussian belongs to the static background. These attributes are then frozen for the remainder of the sequence.

In subsequent frames, only the 3D centers (x_t, y_t, z_t) and 3D rotations $(q_{w,t}, q_{x,t}, q_{y,t}, q_{z,t})$ of the gaussians are updated, enabling motion. In other words, each gaussian is treated as a persistent attribute of an object that existed in the first frame.

Physically-Inspired Regularization Losses Fixing only the appearance-related attributes (color, opacity, size) is not sufficient to ensure accurate gaussian tracking, especially in textureless or ambiguous regions. Therefore, the optimization process is constrained using three physically-based priors:

1. Local Rigidity Loss This term encourages nearby gaussians to move as if part of a locally rigid body between consecutive frames:

$$\mathcal{L}_{\text{rigid}} = \frac{1}{k|\mathcal{S}|} \sum_{i \in \mathcal{S}} \sum_{j \in \mathcal{N}(i)} w_{i,j} \left\| \Delta \mu_{ij}^{t-1} - \mathbf{R}_{i,t-1} \mathbf{R}_{i,t}^{-1} \Delta \mu_{ij}^{t} \right\|_2 \tag{4}$$

- $\mathbf{R}_{i,t}$: rotation matrix of gaussian i at time t
- $w_{i,j}$: weighting function (e.g., gaussian based on spatial proximity)
- $|\mathcal{S}|$: number of gaussians being considered
- $\mathcal{N}(i)$: the set of the k nearest neighbors of gaussian i, determined based on the Euclidean distance in 3D space.
- $\Delta \boldsymbol{\mu}_{ij}^t = \boldsymbol{\mu}_{j,t} - \boldsymbol{\mu}_{i,t} \in \mathbb{R}^3$ represents the relative position vector from gaussian i to gaussian j at time step t.

2. Rotation Similarity Loss This loss encourages consistent rotation behavior across neighboring gaussians:

$$\mathcal{L}_{\text{rot}} = \frac{1}{k|\mathcal{S}|} \sum_{i \in \mathcal{S}} \sum_{j \in \text{knn}(i;k)} w_{i,j} \left\| \hat{q}_{j,t} \hat{q}_{j,t-1}^{-1} - \hat{q}_{i,t} \hat{q}_{i,t-1}^{-1} \right\|_2 \tag{5}$$

- $\hat{q}_{i,t}$: unit quaternion representing the rotation of gaussian i at time t

This Local Rigidity Loss and Rotation Similarity Loss are applied only between the current and previous timestep.

3. Isometry Loss The isometry loss preserves relative distances between neighboring gaussians across frames to prevent global drift:

$$\mathcal{L}_{\text{iso}} = \frac{1}{k|\mathcal{S}|} \sum_{i \in \mathcal{S}} \sum_{j \in \mathcal{N}(i)} w_{i,j} \left| \left\| \Delta \boldsymbol{\mu}_{ij}^0 \right\|_2 - \left\| \Delta \boldsymbol{\mu}_{ij}^t \right\|_2 \right| \tag{6}$$

- This penalizes deviations from the original pairwise distances defined at frame $t = 0$, helping maintain structural consistency.

Each of these loss terms contributes to a robust and physically plausible deformation of the gaussian field over time.

Densification Step The densification step is applied only during the optimization of the initial frame. Consequently, the number of Gaussians whose motion will be approximated throughout training is entirely determined by this initial stage.

Densification relies on the accumulation of 2D Gaussian gradient magnitudes computed across all training views. These gradients are accumulated over multiple passes - each corresponding to one training iteration per view - which enhances robustness by capturing consistent patterns of novelty observable from multiple viewpoints.

This strategy allows the method to identify regions where visual changes are prominent across views and to perform Gaussian splitting or cloning in those areas. As a result, it improves scene coverage in parts that are underrepresented but spatially coherent across multiple perspectives.

4. Proposed Method

4.1. Overview

The proposed method builds upon 3DGStream but can be generalized to other dynamic Gaussian Splatting approaches, as many of them share a common pipeline involving new object or under-reconstructed region detection and a reconstruction algorithm based on the 3D Gaussian Splatting method [2].

The core mechanism tracks the gradients of Gaussian view-space positions after the first-stage optimization. In the second stage, a densification step is performed based on the magnitude of these view-space gradients. This allows the system to identify regions where new objects appear or where reconstruction is poor due to low-frequency textures (e.g., uniform color areas), which often lead to overly large Gaussians that fail to capture detail. The latter case is considered out of scope for this work.

Limitations of original method In the original 3DGStream implementation, the Gaussian densification threshold is set to 0.00015. However, this value proved too high for the Meetroom dataset, where both object motion and new content are subtle compared to the scale of the scene representation. As a result, these under-reconstructed regions were not detected. Lowering the threshold to 0.00007 allowed the method to successfully capture these regions.

Another limitation of the original setup is the Gaussian spawning ratio. The default 1:1 ratio (i.e., one new Gaussian per selected point) may be sufficient for representing fluid or fire-like motion, but it is inadequate for reconstructing solid, rigid objects. To address this, the spawning ratio was increased to 1:15.

Those two shortcomings - namely the overly high densification threshold and insufficient Gaussian spawning rate - are key reasons for the method's limited performance. Additionally, they highlight a broader limitation of the underlying algorithm: its sensitivity to hyperparameters and lack of adaptability across different scenes.

Attention-Aware Loss Another significant issue lies in the loss function design. The original method employs a structural similarity (SSIM)-based loss computed over the entire image frame. However, in scenes such as Meetroom, where the target object (e.g., a phone) occupies only a small portion of the frame (approximately 0.25% of the image area), reconstruction errors in that region contribute minimally to the overall loss. This leads to weak supervision

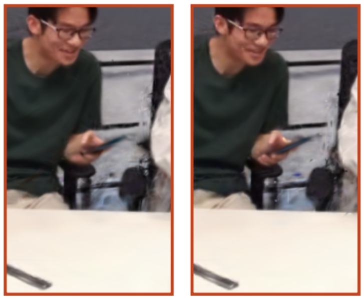

Figure 5. Comparison of loss types: (a) global loss (2), (b) attention-aware loss (10).

and fails to encourage meaningful corrections in localized, high-interest regions.

To address this, we propose an attention-aware loss function that supplements the global loss with a local component focused on regions of interest. These regions are defined using binary masks (7) that identify the appearance of new objects or under-reconstructed areas.

$$I^{\text{mask}} = I \odot \mathcal{M}, \qquad I^{\text{mask}}_{\text{gt}} = I_{\text{gt}} \odot \mathcal{M} \tag{7}$$

The local patch loss is defined as:

$$\begin{aligned} \mathcal{L}_{\text{local}} = \frac{1}{|\mathcal{M}|} \Big[(1-\lambda) \left\| I^{\text{mask}} - I^{\text{mask}}_{\text{gt}} \right\|_1 \\ + \lambda \left(1 - \text{SSIM}(I^{\text{mask}}, I^{\text{mask}}_{\text{gt}})\right) \Big] \end{aligned} \tag{8}$$

The global loss over the full image is:

$$\mathcal{L}_{\text{global}} = (1-\lambda) \cdot \|I - I_{\text{gt}}\|_1 + \lambda \cdot (1 - \text{SSIM}(I, I_{\text{gt}})) \tag{9}$$

The final total loss combines both terms:

$$\mathcal{L}_{\text{total}} = \mathcal{L}_{\text{local}} + \mathcal{L}_{\text{global}} \tag{10}$$

When the loss focuses attention on the reconstruction of the evaluated region, the quality of reconstruction significantly improves, as illustrated in Figure 5.

Criterion for Mask Selection The choice of patch locations for the attention mask is crucial to the effectiveness of the localized loss. In our setting, we define five square patches of size 128×128 pixels, which we found sufficient to cover the most critical regions requiring focused optimization. Placing greater emphasis on regions associated with new objects increases the likelihood that these objects will be accurately reconstructed during the optimization process.

Patch centers are selected from the spatial distribution of newly spawned Gaussians using the following strategy:

Given a set of 3D positions $\{\mathbf{x}_i\}_{i=1}^N \subset \mathbb{R}^3$, we apply a greedy algorithm to select up to k patch centers that satisfy the following criteria:

- Each selected point is at least a distance $d_{\min}$ from all previously selected points.

We initialize the set of selected patch centers:

$$\mathcal{S} \leftarrow \emptyset$$

Then, for each $j = 1$ to N, we proceed as follows:

$$\text{If } \forall \mathbf{x} \in \mathcal{S},\ \|\mathbf{x}_j - \mathbf{x}\|_2 \geq d_{\min}, \quad \text{then } \mathcal{S} \leftarrow \mathcal{S} \cup \{\mathbf{x}_j\} \tag{11}$$

The selection terminates once $|\mathcal{S}| = k$, or all candidates have been exhausted.

Color Difference Map To better detect under-reconstructed regions, we introduce a *color difference map*. Since Gaussian color parameters are fixed after the first-stage optimization, any color mismatch left unresolved during this stage is unlikely to be corrected later—unless explicitly targeted during the densification step.

To compute the color difference map, we compare a rendered image I from a randomly selected training camera with its corresponding ground truth image I_{gt}. For each pixel, we calculate the L2 distance across RGB channels:

$$D(x, y) = \|I(x, y) - I_{\text{gt}}(x, y)\|_2 \tag{12}$$

To suppress minor differences and normalize the result, we define the final distance map as:

$$\hat{D}(x, y) = \frac{\max\left(D(x, y) - \tau,\ 0\right)}{\max_{x,y} D(x, y) + \varepsilon} \tag{13}$$

To identify Gaussians responsible for high-error regions, we render the scene with each Gaussian splatted as a point. Then we sample pixels from the distance map where the normalized error exceeds a threshold τ (e.g., $\tau = 0.4$) and trace back to the Gaussians contributing to those areas.

The Gaussians identified through this setup are selected for densification and passed as candidates for the centers of the patches defined in the mask selection step.

Dynamic Spawning We proposed a *dynamic Gaussian spawning strategy* based on the color error map. The number of Gaussians spawned at each location is made proportional to the local reconstruction error:

> The greater the color discrepancy, the more Gaussians are spawned in that region.

This approach aims to improve reconstruction in regions where no Gaussians currently model rigid and opaque structures - areas that would otherwise remain under-reconstructed. At the same time, it should avoid oversampling regions that exhibit high error due to motion blur or rapid scene changes, where no consistent underlying structure is present.

4.2. Additional Notes

Dynamic Spawning with gradients We evaluated dynamic Gaussian spawning based on the magnitude of Gaussian gradient vectors, but the results were slightly inferior compared to using color difference maps. However, this approach proved beneficial in suppressing the addition of Gaussians in regions without objects, thereby reducing the occurrence of flying Gaussians. Importantly, it still preserved accurate representation of the actual objects.

Clustering of Gaussians for Patch Identification Rather than selecting gaussians for patches centers solely based on their individual spatial proximity, we experimented with a clustering approach. The goal was to identify centers of groups of gaussians that should undergo densification.

While conceptually promising, this approach did not yield better results. It was highly sensitive to clustering hyperparameters - such as the distance threshold for cluster membership and the minimum number of points per cluster - and often failed to robustly generalize across frames. As a result, we chose to abandon clustering-based densification.

Moreover, this step was found to be somewhat redundant: we already enforce spatial separation between newly chosen patches, making additional clustering unnecessary. If the patch size exceeds the actual size of under-reconstructed regions, clustering offers no additional benefit.

5. Results

5.1. Quantitive Comparison

All three methods were trained on a dataset prepared according to the specifications outlined by the original authors. In most cases, this required separate processing for the first frame and subsequent frames.

The reported PSNR values indicate that all three methods achieve similar reconstruction quality, consistent with the results presented in their respective papers.

These results suggest that the majority of the scene was reconstructed successfully and with high fidelity. The HiCoM method achieves significantly lower storage requirements, highlighting a key improvement in efficiency compared to other approaches.

Method	**PSNR** $\uparrow$ (dB)	**Storage** $\downarrow$ (MB)
3DG-Stream	23.85	7.60 / 7.66*
HiCoM	25.11	0.21 / 0.25*
Dynamic Gaussians	24.49	7.34
Improved 3DG-Stream	<u>23.89</u>	7.6 / 7.66*

Table 1. **Evaluation on the distorted dataset.** * Indicates per-frame storage when including the initial point cloud.

Improved 3DG-Stream achieves only a slightly higher PSNR compared to the original version. Although the reconstruction of the phone is more detailed and visible in more frames than in the baseline, this improvement comes at a cost: for every new Gaussian added, one is removed. As a result, the method may under-reconstruct some uniform regions, ultimately balancing out the PSNR and failing to fully reflect the improved reconstruction quality. Furthermore, since the phone occupies only a small portion of the scene, its contribution to the overall PSNR metric is limited.

HiCoM achieves the highest PSNR, likely due to its accurate reconstruction of static background regions that closely match the ground truth. However, a closer inspection reveals that the method introduces a significant amount of noise in areas corresponding to moving objects. This noise suggests poor handling of dynamic content, which is an undesirable characteristic of the algorithm despite its strong performance on static regions.

It is worth noting that the training time for 3DG-Stream and HiCoM was significantly shorter - by a factor of approximately 6 - compared to Dynamic Gaussians, making them more efficient for practical use.

5.2. Qualitative Comparison

Eventhough all the methods yield satisfactory results in terms of metrics, it is impossible to tell if our evaluation objective was met. To gain comprehensive insight into quality of new object reconstruction in the rendered frames from test camera.

3DGStream The emerging object - a phone - fails to be reconstructed, indicating a shortcoming in Stage 2 of the optimization process, which is designed to account for new objects appearing in the scene. Stage 2 relies on detecting high view-space positional gradients to localize under-reconstructed regions. However, in this case, the phone is small, blue in color, and partially blends with a green T-shirt background. Its motion is also minimal. These combined factors likely result in positional gradients that are too weak

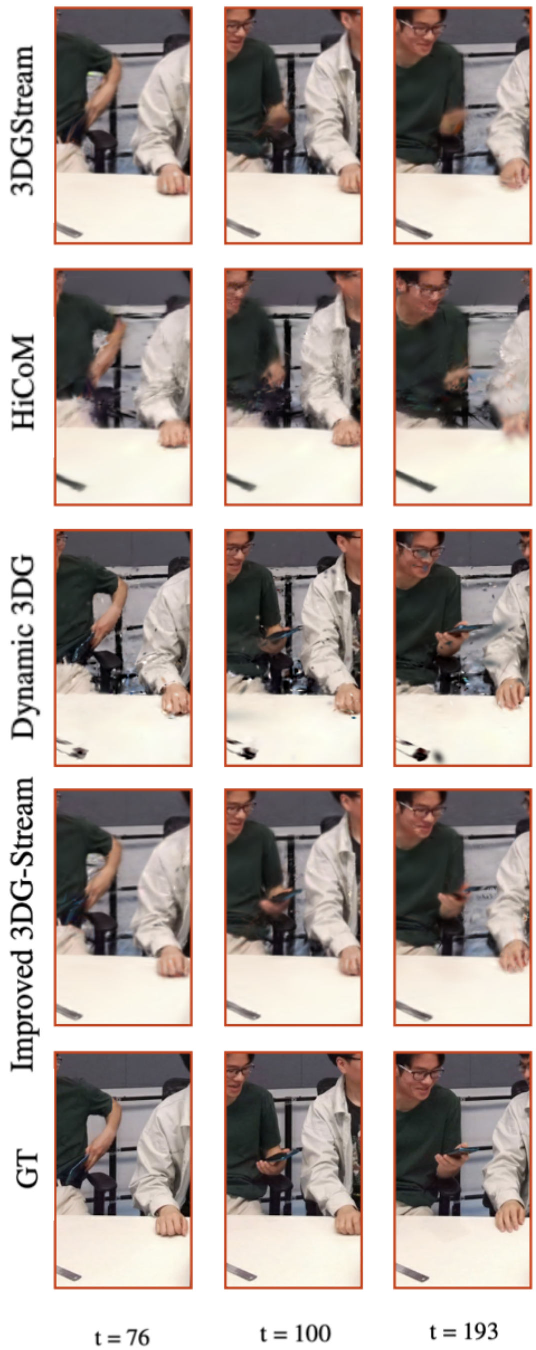

Figure 6. Cropped renderings of selected frames from test camera 0 on the Meetroom dataset.

to surpass the threshold required for new Gaussian spawning. As a result, the model does not recognize this region as requiring additional representation.

HiCoM Similar to 3DG-Stream, HiCoM also fails to reconstruct the phone. However, the underlying reasons are fundamentally different. The method does not incorporate any explicit mechanism for detecting or modeling newly emerging objects in the scene. Its Continual Refinement stage only densifies existing gaussians by duplicating or splitting them in regions identified as underrepresented—typically based on local rendering error. Since new gaussians can only be created through refinement of already existing ones, the model cannot represent objects that were entirely absent in the first frame. If no gaussians were initially placed in the region where the phone appears, there are no anchor points for refinement, and the phone cannot be reconstructed.

The visual artifacts around moving individuals are likely due to limitations of the Coherent Motion model. The hierarchical motion estimation operates over spatial partitions and applies shared transformations, which may be too coarse to capture fine-grained, per - gaussian movements - especially those involving small or fast-moving body parts like limbs. This highlights a key limitation: although moving objects may occupy a small portion of the scene, they are perceptually dominant. A model focused on gradual, region-level motion may reconstruct static backgrounds well, but struggle to represent the subtle and complex dynamics of foreground motion, leading to unnatural blending or ghosting artifacts.

Dynamic 3D Gaussians In contrast to the previous methods, Dynamic 3D Gaussians successfully reconstructs the phone, despite the authors stating that modeling newly emerging objects is a limitation of their approach. While no new Gaussians are introduced during the main training loop, an excess of them is generated during the densification step applied to the initial frame. The existing ones are allowed to move and rotate freely across frames. Unlike HiCoM, which applies motion in a coarse, region-based manner, Dynamic 3D Gaussians performs motion estimation at the level of individual gaussian. This flexibility enables some gaussians - originally associated with the T-shirt in the first frame - to be displaced toward the region where the phone appears.

This behavior is guided by a combination of physically-inspired regularization losses: local rigidity, rotation consistency, and isometry. These priors ensure that gaussians move in a coherent and physically plausible manner while allowing sufficient flexibility to capture local deformations. Additionally, the phone's color similarity to the surrounding T-shirt may have contributed to the reconstruction, as it allows nearby gaussians with similar appearance attributes to approximate the phone without requiring new gaussians to be added.

To fully assess the limitations of Dynamic 3D Gaussians in modeling newly emerging objects, one would need to evaluate it on a dataset where a new object with distinct color and structure enters the scene - such that no similar gaussians exist nearby in the first frame. In such a scenario, it is likely that the method would struggle to reconstruct the object, just as 3DG-Stream and HiCoM do. This suggests that none of the examined methods provide a complete solution for handling new object emergence in dynamic 3D scenes.

Improved 3DG-Stream The reconstruction of the new object is detailed and does not suffer from under-reconstruction. However, one notable flaw is the flickering effect observed in the output video - the object is not consistently reconstructed in every frame. This issue arises because the difference maps used to identify under-reconstructed regions are computed from a single view. If the object is occluded or not visible in that view, the corresponding region is not flagged for densification, and thus remains under-reconstructed. Conversely, when the object is visible, it is accurately reconstructed, demonstrating that the method behaves as intended when provided with the correct visibility cues.

It is also worth noting that the dynamic spawning mechanism successfully prevents excessive Gaussian spawning in unrelated regions, effectively avoiding artifacts such as "flying Gaussians." Nonetheless, the reliance on view-dependent evaluation remains a key limitation of this approach and should be further addressed in future work.

5.3. Undistorted dataset

Method	**PSNR** ↑ (dB)	**Storage** ↓ (MB)
3DG-Stream	<u>33.30</u>	7.6 / 7.66⋆
HiCoM	24.93	0.31 / 0.35⋆
Dynamic Gaussians	22.73	7.71
Improved 3DG-Stream	<u>33.32</u>	7.6 / 7.66⋆

Table 2. Evaluation on **undistorted dataset** . ⋆ indicates storage per frame with initial point cloud.

3DG-Stream emphasizes the importance of undistorting subsequent camera frames. This process removes lens distortion from the input images and updates the associated camera parameters, resulting in a rectified version of the scene that is more suitable for geometric processing.

To ensure a fair comparison, additional experiments were conducted on the undistorted version of the dataset to assess whether this preprocessing step benefits other methods. However, a significant improvement was observed only for 3DG-Stream, which demonstrated a 39% performance increase. The results for the other methods remained within the standard deviation observed across multiple runs.

5.4. Dynamic 3D Gaussians with Meetroom Dataset

Segmentation The method inherently uses segmentation masks to distinguish between static background and dynamic foreground gaussians. However, in the experiments conducted for this report, segmentation masks were not available. To enable training, all gaussians were assigned to the foreground by setting their background logits to zero. This effectively disables the segmentation-based split that is normally used to prevent losses such as rigidity, rotation similarity, and isometry from being applied between dynamic and static components of the scene.

In the standard setup, several loss terms rely on the segmentation split:

$$\mathcal{L}_{\text{floor}} = \frac{1}{N_{\text{fg}}} \sum_{i \in \mathcal{F}} \max(y_i, 0), \tag{14}$$

$$\mathcal{L}_{\text{bg}} = \frac{1}{N_{\text{bg}}} \sum_{i \in \mathcal{B}} \left(\left\| \mathbf{x}_i - \mathbf{x}_i^{(0)} \right\|_1 + \left\| \mathbf{R}_i - \mathbf{R}_i^{(0)} \right\|_1 \right), \tag{15}$$

$$\mathcal{L}_{\text{seg}} = 0.8 \cdot \text{L1}(\hat{\mathbf{s}}, \mathbf{s}) + 0.2 \cdot (1 - \text{SSIM}(\hat{\mathbf{s}}, \mathbf{s})), \tag{16}$$

- $\mathcal{F}$ and $\mathcal{B}$ denote the sets of foreground and background Gaussians respectively,
- y_i is the Y-coordinate of the i-th Gaussian,
- $\mathbf{x}_i^{(0)}$ and $\mathbf{R}_i^{(0)}$ are the initial positions and rotations of background Gaussians,
- $\hat{\mathbf{s}}, \mathbf{s}$ are the predicted and ground truth segmentation maps.

In experiment setting, where no segmentation masks are used, we omit the background loss $\mathcal{L}_{\text{bg}}$ and segmentation loss $\mathcal{L}_{\text{seg}}$ from the final loss function. This effectively allows all gaussians to move freely across the entire scene. On one hand, this flexibility enables the model to reconstruct new objects such as the phone. On the other hand, it magnifies instability, leading to visible artifacts—commonly referred to as "flying gaussians."

Learning Rates and Loss Balancing Adjusting the weight of the floor loss $\mathcal{L}_{\text{floor}}$ was found to have minimal impact on the suppression of artifacts. In particular, setting this term to zero did not eliminate artifacts, while increasing it too much dominated the total loss and led to degraded overall performance, indicating an imbalance in the optimization dynamics.

Overfitting and Camera Layout A potential contributing factor to the observed artifacts is overfitting to initial frame, particularly in the absence of sufficient view diversity. The Meetroom dataset includes 27 cameras, but they are primarily positioned in front of the subjects, offering limited angular coverage. This sparse view distribution may lead to incorrect 3D placement of gaussians - especially in depth - during the per-frame optimization, as the model may overfit to 2D projections without strong multi-view constraints. Consequently, the excess of gaussians added in densification step based on 2D projected gradients, drifts around the scene, producing visual artifacts such as "flying gaussians."

The initial reconstruction is highly sensitive to the densification process, which proves overly aggressive. Reducing its intensity leads to an oversimplified scene representation that falls short of the requirements for dynamic scene reconstruction. While this reduction helps minimize visual artifacts, it risks excluding regions that require modeling. In particular, further limiting the number of Gaussians eligible for densification may prevent the reconstruction of newly appearing objects - such as a phone - ultimately hindering accurate scene representation.

Lastly, we repeated the same training setup - without segmentation masks - on the Panoptic dataset, which features a more diverse camera layout. In this case, the artifact pattern did not emerge, supporting the assumption that limited view diversity and over densified gaussians contributes to the issue.

6. Conclusion

In conclusion, none of the evaluated methods fully address the challenge of reconstructing new objects that emerge in a scene. **3DGStream** fails likely due to the limitations of its threshold-based detection mechanism, **HiCoM** lacks any explicit strategy to accommodate the appearance of new objects.

Dynamic 3D Gaussians shows some potential in handling emerging objects, but a conclusive assessment is not possible in this study. The method depends on segmentation masks to differentiate between static and dynamic regions; however, such masks were unavailable for the dataset used. Moreover, excessive densification - while enabling the representation of new objects - degrades the overall quality of scene reconstruction by introducing artifacts. This compromises the reliability of the method in dynamic settings.

Improved 3DG-Stream demonstrates that detailed reconstruction of new objects is achievable, offering promising potential for reducing the gap between rendered and ground truth videos caused by under representation of novel content. This highlights the method's capability to reliably reconstruct dynamic 3D scenes. However, it remains sensitive to per-view evaluation, which still poses a limitation. This issue presents a clear direction for future research, and resolving it could lead to a state-of-the-art solution to the challenges introduced by emerging object reconstruction.

7. Future Work

While we present an improved version of 3DG-Stream that achieves better reconstruction of new objects and shows strong potential to generalize across different scenes, there remains considerable room for improvement. The current per-frame representation is highly sensitive to the specific view selected for evaluation. A more robust approach could involve tracking the newly spawned Gaussians, their gradients, or color differences across multiple frames. Future work may explore computing 2D position gradients from multiple views, as inspired by [4], or aggregating multiple difference maps from all training camera views. Such strategies are expected to mitigate the issue of flickering objects, which currently depend heavily on their visibility in individual evaluation views.

Future investigations should utilize datasets in which newly emerging objects have distinct appearances, clearly different from any other objects present in the initial frame. Additionally, datasets should feature more diverse and comprehensive multi-view camera placements that offer better coverage of the scene - particularly from different angles and depths - to ensure robust 3D reconstruction.

Since Dynamic 3D Gaussians relies on accurate segmentation and sufficient depth cues to properly track and reconstruct dynamic elements, future work should explore how this method performs when segmentation masks are available and when camera configurations provide adequate spatial information. These factors are critical for validating whether the method can truly generalize to scenes with emergent objects.

The challenge of reconstructing objects that appear after the first frame is close to being solved. However, current methods - such as 3DG-Stream, HiCoM, and Dynamic 3D Gaussians - each fall short for different reasons. Consequently, future approaches should explicitly incorporate mechanisms for detecting and modeling novel scene elements as they emerge over time, without relying on their presence or visibility in the initial frame, as demonstrated by the Improved 3DG-Stream. Enhancing the robustness and generalizability of such methods will be essential for advancing dynamic scene reconstruction in real-world applications.

References

[1] J. Sun, H. Jiao, G. Li, Z. Zhang, L. Zhao, and W. Xing, "3dgstream: On-the-fly training of 3d gaussians for efficient streaming of photo-realistic free-viewpoint videos," 2024. [Online]. Available: https://arxiv.org/abs/2403.01444 2

[2] B. Kerbl, G. Kopanas, T. Leimkühler, and G. Drettakis, "3d gaussian splatting for real-time radiance field rendering," 2023. [Online]. Available: https://arxiv.org/abs/2308.04079 2, 3, 4, 5

[3] Q. Gao, J. Meng, C. Wen, J. Chen, and J. Zhang, "Hicom: Hierarchical coherent motion for streamable dynamic scene with 3d gaussian splatting," 2024. [Online]. Available: https://arxiv.org/abs/2411.07541 3

[4] J. Luiten, G. Kopanas, B. Leibe, and D. Ramanan, "Dynamic 3d gaussians: Tracking by persistent dynamic view synthesis," 2023. [Online]. Available: https://arxiv.org/abs/2308.09713 4, 10